Geochemistry, Geophysics, Geosystems

RESEARCH ARTICLE
10.1029/2020GC009582

Key Points:

- Mineralogical, chemical, and spectral characterization of a 100 m long drill core into lacustrine sediments from a mafic basin allow for characterization of basin conditions through ~1 Myr of deposition, burial, and diagenesis
- Statistical analyses divide the core record into meaningful zones that reflect changes in basin conditions, with one shift dominated by a river capture event and the other by a diagenetic fluid alteration front characterized by siderite nodule growth
- The primary mineralogical shifts are in Al and Mg silicates and complex Fe-rich phases. X-ray amorphous/nanophase material persists even in the deepest sediment, and contains Fe in both ferric and ferrous forms

Supporting Information:

Supporting Information may be found in the online version of this article.

Correspondence to:

R. Y. Sheppard,
rachel.y.sheppard@jpl.nasa.gov

Citation:

Sheppard, R. Y., Milliken, R. E., Russell, J. M., Sklute, E. C., Dyar, M. D., Vogel, H., et al. (2021). Iron mineralogy and sediment color in a 100 m drill core from Lake Towuti, Indonesia reflect catchment and diagenetic conditions. *Geochemistry, Geophysics, Geosystems*, *22*, e2020GC009582. https://doi.org/10.1029/2020GC009582

Received 3 DEC 2020
Accepted 29 MAR 2021

Iron Mineralogy and Sediment Color in a 100 m Drill Core From Lake Towuti, Indonesia Reflect Catchment and Diagenetic Conditions

Rachel Y. Sheppard[1], Ralph E. Milliken[1], James M. Russell[1], Elizabeth C. Sklute[2], M. Darby Dyar[2,3], Hendrik Vogel[4], Martin Melles[5], Satria Bijaksana[6], Ascelina K. M. Hasberg[5], and Marina A. Morlock[4]

[1]Department of Earth, Environmental, and Planetary Sciences, Brown University, Providence, RI, USA, [2]Planetary Science Institute, Tucson, AZ, USA, [3]Department of Astronomy, Mt. Holyoke College, South Hadley, MA, USA, [4]Institute of Geological Sciences & Oeschger Centre for Climate Change Research, University of Bern, Bern, Switzerland, [5]Institute of Geology and Mineralogy, University of Cologne, Cologne, Germany, [6]Faculty of Mining and Petroleum Engineering, Institut Teknologi Bandung, Bandung, Indonesia

Abstract Iron is the most abundant redox-sensitive element on the Earth's surface, and the oxidation state, mineral host, and crystallinity of Fe-rich phases in sedimentary systems can record details of water-rock interactions and environmental conditions. However, we lack a complete understanding of how these Fe-rich materials are created, maintained, and oxidized or reduced in sedimentary environments, particularly those with mafic sources. The catchment of Lake Towuti, Indonesia, is known to contain a wide range of abundant crystalline Fe oxide, and the lake has a long sedimentary history. Here, we study a ~100 m long drill core from the lake to understand patterns of sedimentation and how young iron-rich sediments are affected by diagenesis through geologic time. We use visible/near infrared and Mössbauer spectroscopy, X-ray diffraction, bulk chemistry measurements, and statistical cluster analysis to characterize the core sediment. We find that the core sediment can be divided into three statistically different zones dominated by Mg serpentine, Al clay minerals, and Fe^{2+} carbonate, respectively. The entire core is rich in nanophase Fe, and elemental correlations and Fe mineralogy vary between these zones. The nanophase Fe is highly complex with both ferrous and ferric components, and contributes to, but does not dictate, variations in sediment color. We propose that the distinctive zones are the result of structural basin changes (notably river capture and shifting drainage patterns), and diagenetic overprinting caused by deep burial of reactive Fe. This complex record has implications for disentangling depositional and diagenetic trends in other mafic lacustrine systems.

1. Introduction

A thick lacustrine sediment succession in Lake Towuti, located on the island of Sulawesi, Indonesia, offers a unique opportunity to study the relationships between tropical environmental conditions, Fe-rich sediment transport and deposition, and biological and sediment diagenetic processes under variable redox conditions through time. The warm, wet, metal-rich, redox-variable conditions of Lake Towuti provide an interesting contrast to other well-studied lakes in mafic terrains that are characterized by colder climates, shallower lake levels, and fully oxidized conditions (Benson & Mahood, 2016; Fristad et al., 2015; Gudmundsdottir et al., 2016; Krivonogov et al., 2012). One of the oldest lakes situated in the Indo-Pacific Warm Pool, Towuti is expected to preserve an important record of basin-scale processes and climatic conditions in this region, a record that can be extracted by detailed study of the inorganic and organic chemistry of sediments within the lake. In 2015, an international team of scientists extracted more than 1,000 m of sediment core from Lake Towuti to investigate environmental change and sedimentation in the lake (Russell et al., 2016). Modern lake bottom sediments in the Towuti system have been the focus of intense study in recent years (Costa et al., 2015; Goudge et al., 2017; Hasberg et al., 2018; Morlock et al., 2018; Sheppard et al., 2019; Vuillemin et al., 2019; Weber et al., 2015), and a recent study by Russell et al. (2020) presented the visual and chemical stratigraphy of a ~160 m long composite sediment core from Lake Towuti to investigate the long-term tectonic and limnologic evolution of the lake. The 203 m deep lake is currently redox-stratified but appears to experience sporadic complete overturn and reoxygenation of the water column that may increase the

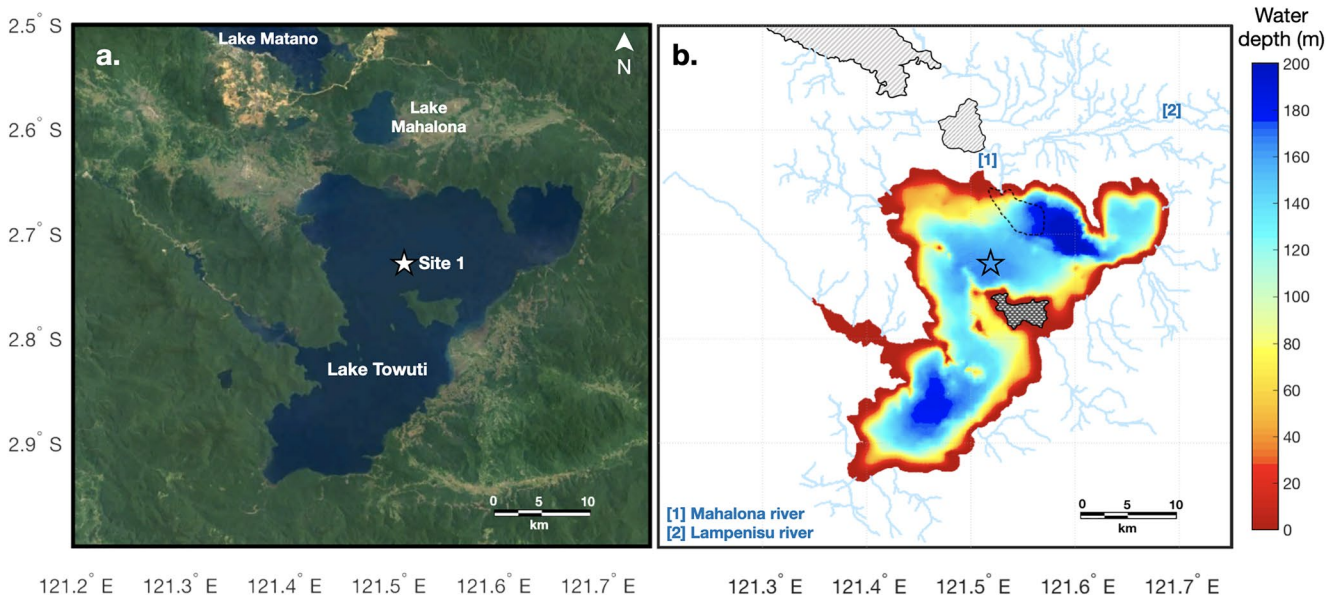

Figure 1. Large lakes of the Malili Lakes System: Lakes Matano, Mahalona, and Towuti. (a) Landsat composite image of the Malili Lakes System, including the southeastern tip of Lake Matano, Lake Mahalona, and Lake Towuti. (b) Bathymetry of Lake Towuti (m). Rivers are in light blue, and the Mahalona and Lampenisu rivers are labeled (1) and (2), respectively. The delta of coarse-grained material carried in by the Mahalona River is outlined by a dashed line. The location of the Site 1 drill core is denoted with a star.

delivery of metals to sediments on the lake bottom, and Russell et al. (2020) highlight how these conditions, as well as the carbon and nutrient biogeochemistry of the lake have evolved through time.

In this study, we build upon and expand that work by focusing on several novel datasets and quantitative analyses of the upper ~100 m of the composite core (Unit 1 of Russell et al., 2020). This includes (a) characterization of dominant clay minerals and their cation chemistry with depth (Al, Fe, and Mg phyllosilicates), (b) statistical chemostratigraphic analysis to objectively identify significant changes in sediment composition, building on the visual stratigraphy of Russell et al. (2020), (e) characterization of Fe mineralogy with depth and how it relates to Fe redox cycling with depth, and (d) quantitative analysis of sediment color and comparison with mineralogy to determine the extent to which color can be used as a reliable proxy for sediment composition. The core data presented here allow for direct comparison with previous studies of the modern sediments to investigate the influences of sediment diagenetic processes operating at depth. Our new record of sediment composition highlights the importance of iron diagenesis to the stratigraphy of Lake Towuti.

2. Background

Lake Towuti is the largest of the five Malili lakes (Figure 1a) and is located in the East Sulawesi Ophiolite, the third largest ophiolite in the world, which is dominated by unserpentinized harzburgite, dunite, and serpentinized lherzolite (Kadarusman et al., 2004). Several rivers drain into Lake Towuti (Figure 1) and supply the lake with high abundances of Fe and other metals such as Cr and Ni (Costa et al., 2015; Kadarusman et al., 2004). The largest tributary, the Mahalona River, enters the lake to the north and delivers sediment that is dominated by serpentines, which are particularly abundant in sand-sized and coarser grains. This serpentine-rich sediment contributes to the build up of a prograding delta with abundant Mg-serpentines that is bound by fault-controlled bedrock highs to the south but extends ~10 km into the 200 m deep basin to the E of the river mouth (Goudge et al., 2017; Vogel et al., 2015).

As is typical in tropical environments, much of the catchment of Lake Towuti has well-developed lateritic soils on top of the bedrock. These soils follow typical chemical and mineralogical zonation of tropical laterites (Colin et al., 1990; Golightly & Arancibia, 1979; Widdowson, 2007) and are rich in Al phyllosilicates and Fe oxides, are very susceptible to erosion and mass wasting events and constitute much of the influx

into the lake via the surrounding rivers (Goudge et al., 2017; Morlock et al., 2018; Sheppard et al., 2019). Despite high Fe content in these soils contain a very small proportion of Fe in amorphous phases and are dominated by crystalline Fe oxy/hydr/oxides (Sheppard et al., 2019). The lake sediment, however, contains approximately even distribution of Fe between amorphous and crystalline phases, and drill core sediment contains more Fe hosted in amorphous phases (Sheppard et al., 2019).

Previous studies of piston cores (~10–20 m), surface sediment samples, and river suspended and bedload samples revealed that the mineralogy of surface sediment in Lake Towuti is variable across the lake bottom, with changes dominated by variations in the abundance of predominantly Fe, Mg, and Al phyllosilicates (Goudge et al., 2017; Hasberg et al., 2018; Morlock et al., 2018; Sheppard et al., 2019; Weber et al., 2015). This study has revealed important variations in sediment mineralogy, chemistry, and grain size during transport and deposition within Lake Towuti (Hasberg et al., 2018; Morlock et al., 2018; Sheppard et al., 2019), and highlighted in particular the importance of the Mahalona River, which delivers coarse, Mg-serpentine rich sediment to the lake's northern basin. Analyses of the piston cores revealed strong correlations between mineralogy and grain size, with changes in mineralogy over the last ~40 kyr reflecting variations in the dominant grain size that was deposited over that time. Specifically, finer-grained sediment enriched in aluminous clay minerals transitioned to coarser-grained sediment enriched in Mg-serpentine, driven by lake level changes and migration of the Mahalona River delta (Goudge et al., 2017; Morlock et al., 2018; Vogel et al., 2015). Sediment in the piston cores also showed variations in the abundance of Fe_{total} and redox-sensitive trace elements that are consistent with redox-driven changes in sediment geochemistry during climatically drier periods (Costa et al., 2015). Seismic data of the upper 150 m of basin fill were also collected during the reconnaissance effort and showed an upper lacustrine unit that is underlain by fluvio-lacustrine material, with little evidence of widespread tectonic deformation (Hafidz et al., 2018; Russell & Bijaksana, 2012).

Motivated by the results of these studies, the Towuti Drilling Project (TDP) was conducted in 2015 to collect deeper drill-cores from the lake bottom (Russell et al., 2016, 2020). The longer core samples provide a means to assess environmental processes as a function of deeper time, as well as microbial and diagenetic processes occurring at depth in this ferruginous system. This study focuses on the detailed mineralogical and chemical variations as a function of depth, particularly of the Fe-rich phases. Over 1,000 m of sediment core were recovered from three sites, the deepest reaching bedrock at 162.8 m below the lake floor, and characteristics of a composite core are described in Russell et al. (2020). Major characteristics include basal sediments dominated by silts and sands, overlain by a 2.5 m thick woody peat layer at 100 m depth, reported here as meters composite depth (mcd), and an upper 100 m of alternating thinly bedded red and green clay-sized sediment with localized turbidites, tephras, and diatomaceous oozes (Russell et al., 2016). The upper 100 m correspond to Unit 1 described in Russell et al. (2020) and are the focus of this study. Of the three sites drilled by the TDP, the sediments from only Site 1 (Figure 1) are the focus of this study. Example images of the major lithotypes in this core can be seen in Figure S4.

The alternating pattern of red and green clays has been interpreted to reflect variations in bottom water oxygenation in Lake Towuti as a function of time (Costa et al., 2015; Russell et al., 2020). Specifically, the green clay beds are enriched in organic matter and were interpreted to have been deposited during warmer, wetter periods when the lake was stratified, resulting in anoxic and ferruginous bottom waters. In contrast, the red clay beds contain siderite ($FeCO_3$), low organic matter concentrations, and are interpreted to represent cooler, drier periods when the lake was well-mixed with at least periodically oxygenated bottom water (Russell et al., 2020). The latter condition can result in an increased delivery and/or accumulation of highly reactive iron (e.g., Fe^{3+} in amorphous or poorly crystalline phases) to the lake bottom, which is then reduced at shallow depths in the sediment column to produce siderite, as well as magnetite and other Fe phases (Russell et al., 2020; Vuillemin et al., 2019). However, previous studies have demonstrated that the host phases of Fe in Lake Towuti sediments and the oxidation states of those phases are varied and complex, and that, at least in the modern lake, the concentration of sedimentary Fe does not increase under water column oxygenation (Sheppard et al., 2019). Furthermore, while oxidized Fe is often reddish in color, color is not always a strong proxy for Fe oxidation state; nontronite, for example is a ferric smectite but is commonly green in color (Harder, 1976). As such, additional detailed studies of the mineralogy and chemistry of the drill core samples are needed to evaluate the controls on sediment stratigraphy.

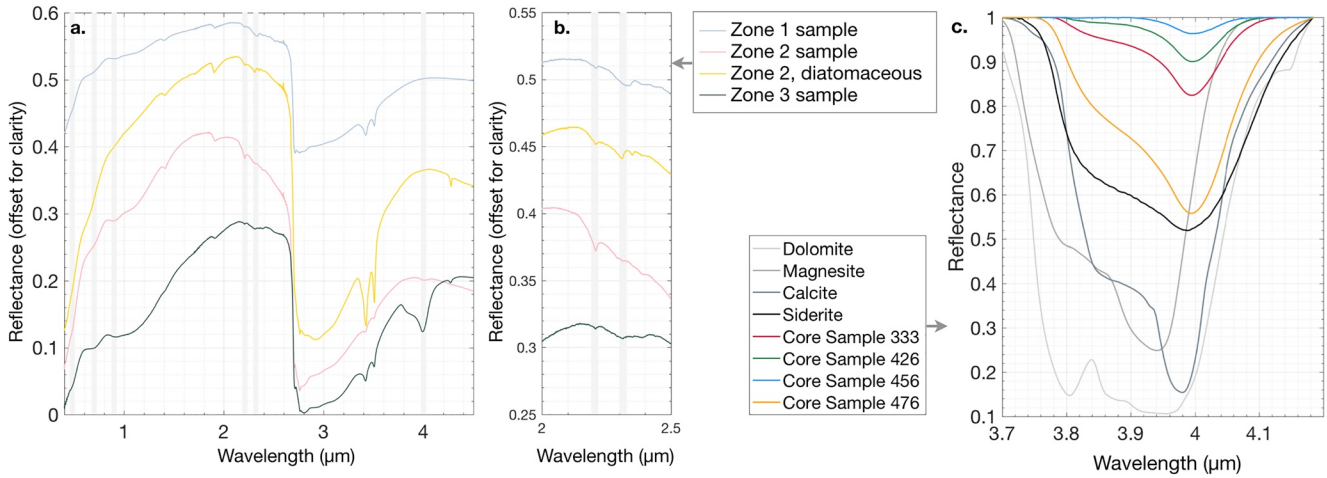

Figure 2. (a) Example spectra from Zones 3, 2, and 1 with relevant bands highlighted. (b) Zoom view of the clay absorption bands. (c) Continuum-removed spectra of the 4.0 μm CO_3 band in several carbonates (gray to black lines) and four core samples with a range of carbonate content (colored lines).

This study characterizes trends in mineralogy and chemistry in the 100 m-long sediment succession of Unit 1 (as defined by Russell et al., 2020) in the composite core and how these relate to sediment source, water column conditions, and diagenetic processes within Lake Towuti, with an emphasis on Fe phases. Sheppard et al. (2019) discussed the importance of early diagenesis and Fe mobilization in the modern surface sediments and showed that movement of iron-rich detritus through the Lake Towuti system resulted in the transformation of crystalline ferric oxides (e.g., hematite, goethite) to Fe-rich X-ray amorphous phases. We examine if similar changes are observed in sediments from the Towuti core.

3. Methods

3.1. Sampling

The three drill cores acquired by the TDP in 2015 were housed and later subsampled at the LacCore facility at the University of Minnesota in 2015/2016. Subsamples were 2–4 cm^3 in volume and taken every ~0.5 m. Wet samples were placed in small plastic containers and kept frozen until they could be freeze dried for analysis. The core samples analyzed for this study are from the 99% complete TDP Site 1 core composite; for additional details on sample collection procedures and processing we refer the reader to Russell et al. (2020). The 185 composite core samples discussed here represent a depth range from 0 to 97 mcd. Additional details on the composite core, sampling strategy, and drilling project are provided by Russell et al. (2016) and Russell et al. (2020). Sample depth and borehole location are presented in Table S1.

3.2. Reflectance Spectroscopy

Reflectance spectra were acquired for dried, powdered sediment samples over a wavelength range of 0.35–4.75 μm using a combination of spectrometers in the NASA Reflectance Experiment Laboratory facility housed at Brown University. An Analytical Spectral Devices (ASD) FieldSpec3 spectroradiometer was used for the visible-near infrared (VNIR, 0.35–2.5 μm) wavelength range and a Thermo Nexus 870 FTIR spectrometer was used for the near-infrared to mid-infrared (NIR-MIR, 0.8–4.75 μm) range. ASD reflectance spectra were acquired relative to a white Spectralon reflectance standard from Labsphere, whereas FTIR reflectance data were acquired relative to diffuse gold. The two sets of spectral data were spliced together at 1.7 μm to provide a continuous spectrum. Example spectra from four samples within the composite core are displayed in Figure 2a, with relevant absorptions highlighted.

A commonly used analysis method in reflectance spectroscopy is to calculate the strengths of diagnostic absorption features. The resulting "band depth" values are a measure of the reflectance values associated with a characteristic absorption feature relative to the reflectance value that would be expected in the absence

of that feature (Clark & Roush, 1984). Band depth values thus range from 0 (absence of an absorption) to 1 (complete absorption/band saturation). The core samples analyzed here were of similar particle size and were also ground before analysis to minimize the effect of particle sizes on spectral reflectance characteristics including albedo. Therefore, relative variations in band depth values are expected to mimic relative abundances of the absorbing species (e.g., minerals). The major mineral phases considered in the spectral analysis were guided by the results of Sheppard et al. (2019) for the lake surface sediments and are discussed below.

3.2.1. Mg Serpentine

Trioctahedral Mg phyllosilicates in the serpentine group (e.g., antigorite, chrysotile, and lizardite) were identified based on an asymmetric absorption centered at ~2.32 μm caused by vibrations (combination bend and stretch) of the Mg-OH bond (Weber et al., 2015).

3.2.2. Al Clay Minerals

Narrow absorptions with minima near ~2.2 μm are caused by combination stretch and bend vibration modes of Al-OH. The presence of two narrow and partially overlapping absorptions with minima at 2.16 and 2.21 μm is most consistent with Al-OH vibrations in kaolinite, whereas other Al-bearing phyllosilicates (e.g., montmorillonite, illite, and muscovite) exhibit a slightly broader symmetric absorption centered near 2.21 μm (Bishop et al., 2008; Clark et al., 1990; Goudge et al., 2017; Weber et al., 2015).

3.2.3. Fe Absorptions

The presence of $Fe^{2+/3+}$ in octahedral and tetrahedral coordination can give rise to a wide range of complex and sometimes overlapping absorptions in the 0.35–2.5 μm range due to electronic absorptions such as intervalence charge transfer, oxygen-metal charge transfer, and crystal field splitting (Burns, 1993). Features associated with $Fe^{2+/3+}$ in oxides and poorly crystalline materials of interest to this study include absorptions at 0.48, 0.7, and 0.9 μm.

3.2.4. Carbonate

A strong CO_3 absorption ($v_1 + v_3$ vibration mode) that consists of several partially overlapping features is located at 3.8–4.0 μm (Gaffey et al., 1993; Sutter et al., 2007). The weaker overtones of these absorptions that occur at shorter wavelengths (e.g., 2.3–2.5 μm) may also be observed when carbonate is abundant.

3.3. X-Ray Diffraction

Powder X-ray diffraction (XRD) measurements were carried out on 40 samples to provide mineralogy for comparison with phases identified in the spectral reflectance data and to provide information on minerals that are not readily detected at VIS-NIR wavelengths (e.g., quartz and feldspar). Dried, powdered samples were analyzed on a Bruker D2 Phaser XRD unit with a Cu Kα source. Sample cups were filled without packing and a flat surface created using a glass slide to minimize introducing a preferential orientation. Measurements were taken from 5° to 90° 2θ at ~0.02° step size and data were analyzed with the ICDD database for phase identification. These XRD results are semi-quantitative as the samples were not spiked with an internal standard.

3.4. Mössbauer Spectroscopy

Mössbauer spectra were collected for a small set of drill core sediment samples to aid in the identification of Fe-bearing phases. The core sediments analyzed with this method were from depths 2.36, 7.72, 14.78, 26.52, 27.12, 30.16, and 75.84 mcd. Mössbauer is a useful tool for distinguishing between Fe oxides in complex samples because the spectra record small energetic changes around Fe atoms. Mössbauer spectra were collected with the sample at 4, 130, and 295 K on a Web Research Co. (now See Co.) W100 spectrometer using a ~75–65 mCi ^{57}Co source in rhodium. Low-temperature spectra were obtained using a Janis Research Co. Model 850 4 K closed-cycle helium compression system. The resulting Mössbauer spectra were fit using the Mex_disd program. These fits can be used to determine various Mössbauer parameters related to Fe valence state and coordination environment (Dyar et al., 2006). Important parameters include the isomer shift (IS),

which is related to the s-electronic charge density that is affected by bond characteristics, valence state, and coordination environment. This shift is shown in Mössbauer spectra as a velocity (mm/s) shift relative to α-Fe foil. Quadrupole splitting (QS) of nuclear energy levels is also determined, which creates the distinctive doublets and sextets seen in Mössbauer spectra. Changes in Fe valence state or changes to the crystal lattice that affect the coordination or bonding environment will affect this splitting and consequently the shape and position of the observed doublets and sextets. Spectra are acquired with samples at multiple temperatures to aid in distinguishing ferrous and ferric Fe, as composition and grain size affect the temperature at which the spectral shape transitions from doublet to sextet.

3.5. Elemental Abundances

Major elements (Al, Ca, Cr, Fe, K, Mg, Mn, Na, Ni, P, Si, and Ti) were analyzed in 185 composite core samples. Elemental abundances were determined using inductively coupled plasma-atomic emission spectrometry (ICP-AES). These results have been published previously by Russell et al. (2020).

3.6. Color

The color of the wet samples was assessed both qualitatively and quantitatively. At the wet stage, images were acquired of each newly cut wet core section by the LacCore core logger; each core section was evaluated visually for red and green horizons forming the qualitative color data set. For a quantitative analysis of color, white-balanced images of the wet cores were used to extract red, green, and blue channel values. These RGB values were processed using a custom Matlab script to assign a color of red or green. Redness is calculated as R/(R + G + B) and greenness is calculated as R/(R + G + B); if Redness > Greenness, the sample is classified as qualitatively red, and vice versa. This calculation was based on portions of LacCore-collected images corresponding to the specific depth and core section. Quantitative and qualitative color of the dried samples were also measured (Figure 3) for each sample, taking care to avoid areas of obvious surface oxidation.

3.7. Statistical Analyses

Structural break analysis was used to determine if data for the core samples could be divided into multiple distinct clusters, hereafter referred to as Zones. This method identifies "breakpoints" via deviations from stability in a classical linear regression model (Bai & Perron, 1998, 2003). The breakpoints are the locations in a timeseries (depths within the composite core in this case) where the regression intercept changes from one stable regression to another. This method requires specifying the number of breakpoints; to do this we use the Bayesian information criterion (BIC) and residual sum of squares (RSS). The advantage of the BIC is that it includes a term to penalize overfitting the data, thus we primarily use BIC to choose the optimal number of breakpoints. We use this method to estimate the breakpoints in the spectral (band depth) data because it results in the most complete data set (i.e., no missing values). Each variable (band depth for a particular mineral or absorbing species) is broken into the most appropriate number of zones independently of the other variables.

4. Results

4.1. Elemental Abundances, Spectral Parameters, and Resulting Statistical Analyses

The primary variations in the composite core can be described in terms of (a) variations in bulk mineralogy as detected using VNIR spectroscopy and XRD, and (b) associated variations in bulk elemental chemistry. Significant changes in mineralogy and chemistry are observed at similar depths in the composite core, consistent with the inherent coupling between these characteristics in the sediments of Lake Towuti. Mineralogical changes are dominated by variations in the relative abundance of serpentine, aluminous clay minerals, and carbonate, whereas chemical variations are dominated by changes in the amount of Mg, Al, and Fe (Figure 4). The overall stratigraphy we observe closely tracks that documented in the chemical and visual stratigraphy by Russell et al. (2020).

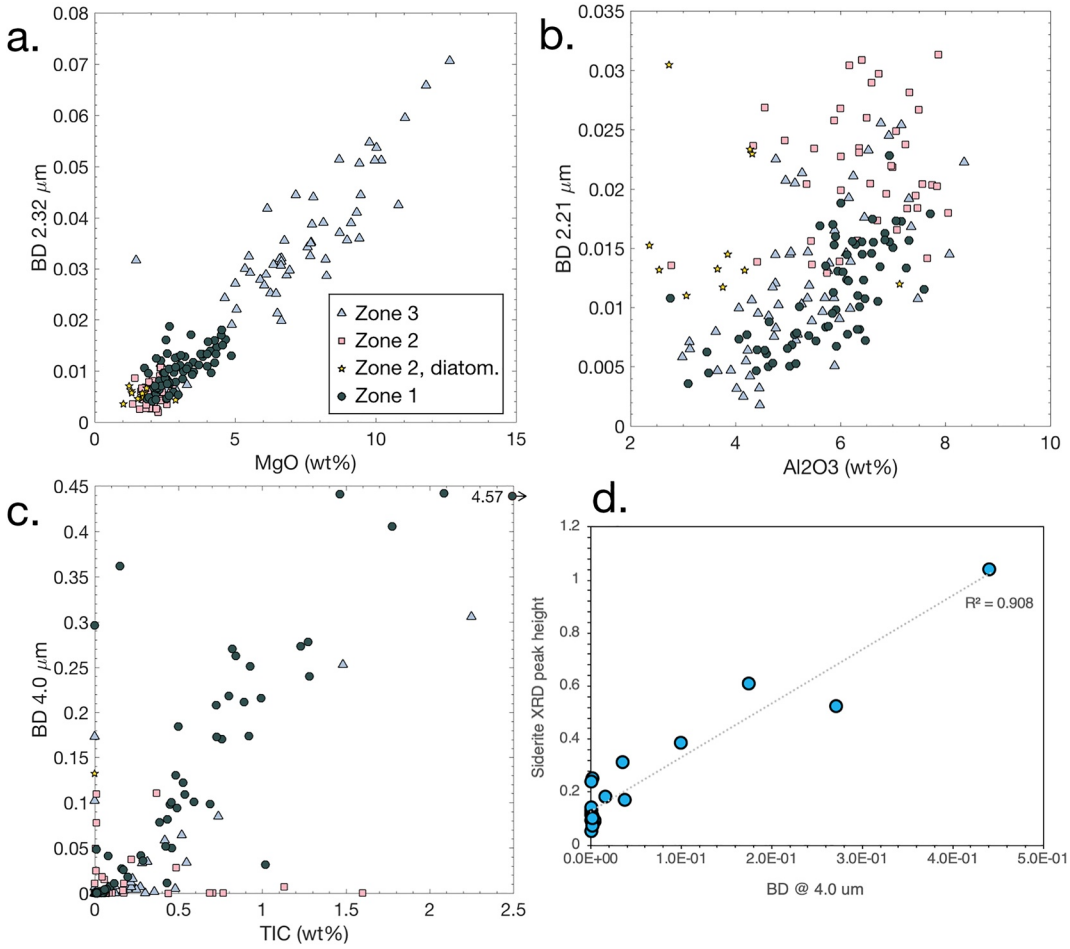

Figure 3. Scatter plots showing the relationship between spectral characteristics and elemental abundances of (a) Mg serpentine, (b) Al clay minerals, and (c) carbonate. (d) Correlation of XRD siderite peak height with the band depth of the 4.0 μm absorption, supporting identification of the carbonate as siderite. For (a–c), dark circles are Zone 1, stars are Zone 2 "diatomaceous," pink squares are Zone 2 "non-diatomaceous," and purple triangles are Zone 3.

These variations are qualitatively apparent in the VNIR, XRD, and ICP data, but the structural break analysis that was applied to the spectral data also reveals three distinct zones in the upper 100 m of the core (Figures 2 and 3). The appropriate number of breakpoints was selected for each spectral parameter using the BIC and RSS approaches (Supporting Information, Figures 1 and 2). The band depth values as a function of sediment depth, which is similar to a time series, was then used to determine the positions (depths) associated with those breakpoints. Analysis of the 2.21 μm Al-OH (aluminous clay mineral) band reveals two breakpoints at depths of 25.8 and 63.2 m, the 2.32 μm Mg-OH (serpentine) band reveals two breakpoints at 26.6 and 69.3 m depth, and the ~4 μm carbonate band reveals one estimated breakpoint at 61.7 m depth (Figure 3). Based on these results, we define depths for Zone 1 as 97–62 mcd, Zone 2 as 62–27 mcd, and Zone 3 as 27–0 mcd. This zonation is similar to the previous zonation of Russell et al. (2020), who defined subunits based on elemental abundances at 0–30, 30–75, and 75–100 mcd depth. Thus, our analysis provides quantitative and mineralogical support for their visual zonation.

Examination of the individual spectra (examples shown in Figure 2) show that samples in Zone 1 (62–97 mcd) are characterized by strong carbonate spectral signatures (in addition to Al-clay minerals such as kaolinite, montmorillonite). Portions of Zone 1 are also visibly enriched in carbonate beds and nodules (Russell et al., 2020), though some areas are devoid of carbonate. The siderite particle size is small (5–10 μm) at shallow depths and increases in deeper sediment forming 0.1 mm to 1 cm mosaic crystals and nodules (Russell et al., 2020; Vuillemin et al., 2019). The carbonate, which is found sporadically throughout

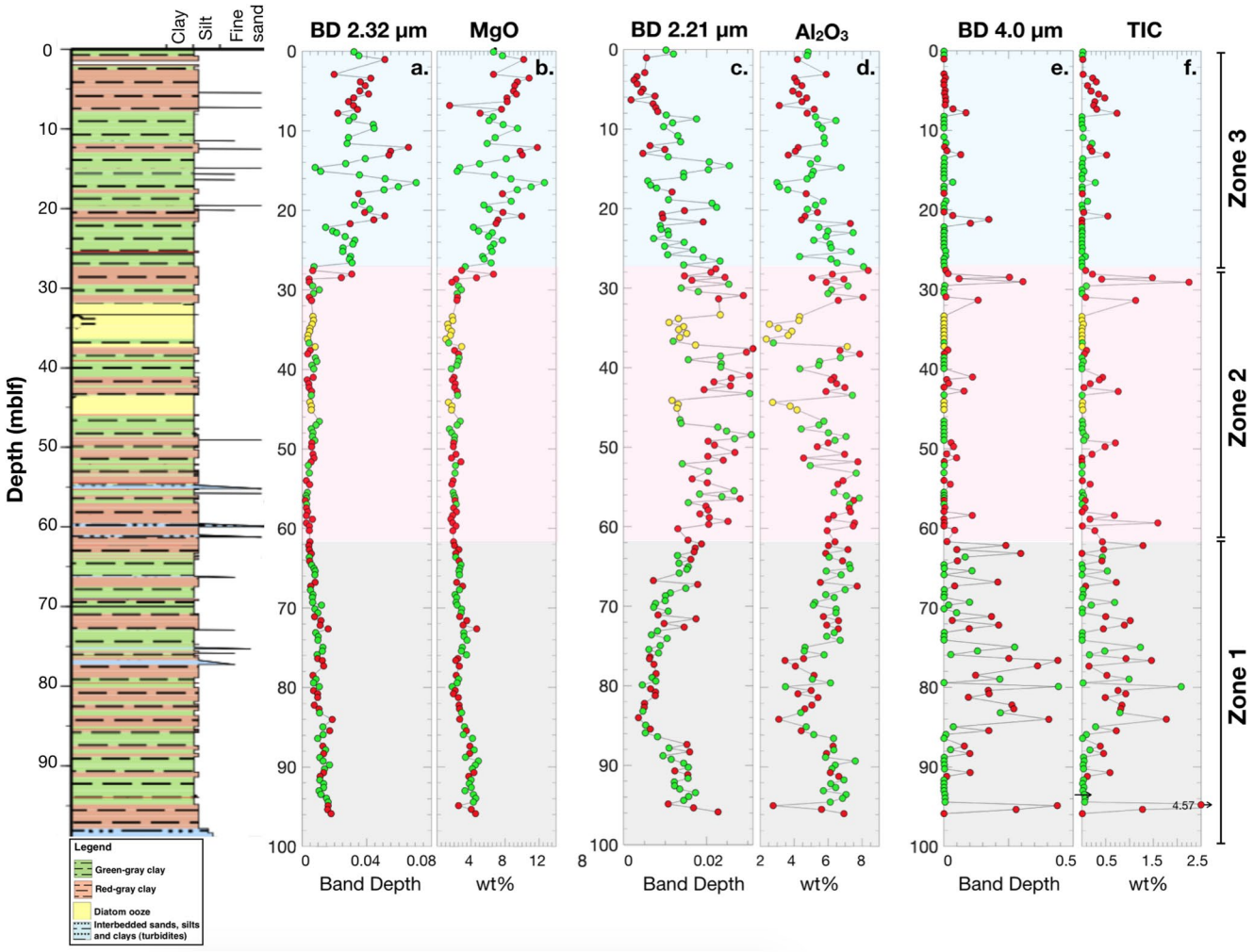

Figure 4. Down-core plots of each core sample's (a) Mg-OH absorption band depth, (b) MgO elemental abundance, (c) Al-OH absorption band depth, (d) Al_2O_3 elemental abundance, (e) CO_3 absorption band depth, and (f) total inorganic carbon. The color of each dot represents the qualitative color of the wet core, determined at LacCore immediately after splitting the core section, with yellow representing pure diatomaceous ooze. Each Zone identified using breakpoint analysis is a different color (Zone 3 blue, Zone 2 pink, Zone 1 gray).

the core and is elevated throughout much of Zone 1, is most consistent with siderite based on the reflectance spectra and XRD patterns. The exact position and shape of the ~4.0 µm CO_3 absorption varies based on the attached cation (Figure 2c, gray lines), and the absorption for siderite occurs at slightly longer wavelengths than other carbonates because of the higher mass of Fe. A broad electronic absorption due to Fe^{2+} in octahedral coordination and with a local minimum near 1 µm is also observed and is consistent with the presence of siderite. The carbonate features seen in the spectra are consistent with siderite regardless of depth (Figure 2c, colored lines), indicating this is the dominant type of carbonate in the core, as has been suggested by Vuillemin et al. (2016, 2020). The spectra of Zone 2 samples are mostly lacking the carbonate features that characterize Zone 1, while spectral features of Fe oxides, Al-clay minerals (e.g., kaolinite, montmorillonite), and lesser Mg-serpentine are more clearly visible. Zone 3 (27-0 mcd) spectra exhibit diagnostic features associated with Mg serpentine. The siderite is commonly in smaller particles in the upper Zones 2 and 3, making it more difficult to detect optically/microscopically compared to the nodules in Zone 1, but easy to observe with XRD and VNIR spectra.

Previous studies of the lake surface and catchment samples demonstrated that VNIR spectral reflectance features could be used as reliable proxies for bulk mineralogy and elemental chemistry (Al, Mg, and to some extent Fe) (e.g., Morlock et al., 2018; Sheppard et al., 2019). As presented in Figure 3 (and Tables S2–S6),

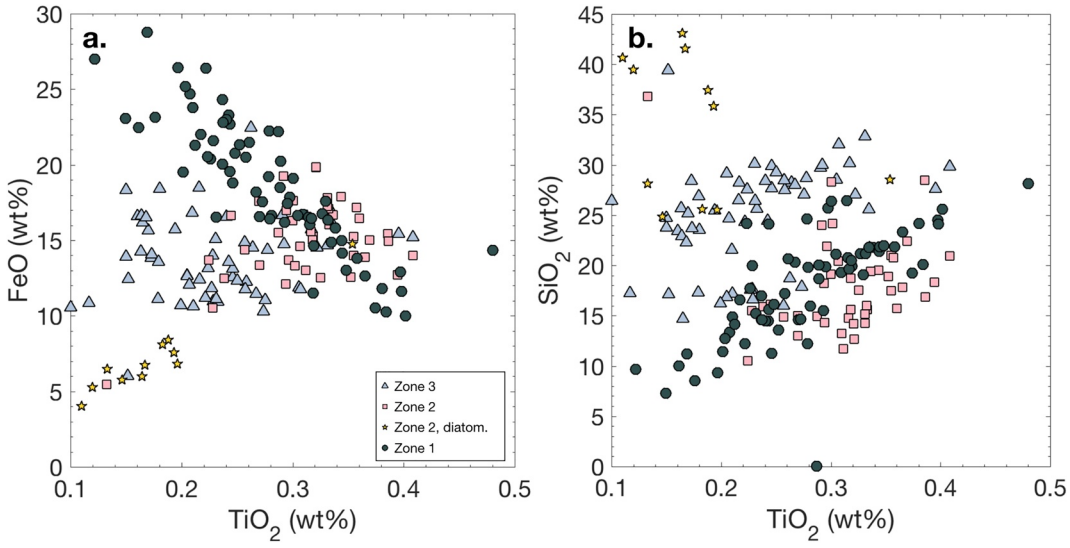

Figure 5. (a) FeO and (b) SiO_2 versus TiO_2 for the three core Zones.

similar trends are observed in the composite core data. There are strong correlations between Mg-OH absorption strength and independently measured Mg, Al-OH absorption strength and Al, and carbonate absorption strength and total inorganic carbon (TIC). This further supports previous results that VNIR reflectance spectroscopy can be used as a rapid, remote technique for qualitative assessment of downcore mineralogy and chemistry (Morlock et al., 2018), as long as the phases present have absorptions in the VNIR wavelength range. In Figure 4, the relevant band depth values are plotted as a function of sample depth. Qualitatively, the spectral and chemical measures are similar to each other. As an example, both MgO and band depth (BD) of the 2.32 μm Mg-OH absorption gradually decrease to almost zero from 16 to 26 mcd. Similarly, both TIC and band depth of the 4.0 μm feature increase near 62 mcd.

Quantitatively, the spectral and chemical data are indeed correlated for all three Zones (Figure 3). MgO abundance and the band depth at 2.32 μm are strongly correlated in Zones 3 and 1 (positive coefficient significant at $p < 0.01$) and correlated in Zone 2 (positive coefficient significant at $p < 0.1$). Al_2O_3 and the band depth at 2.21 μm are strongly correlated (positive coefficient significant at $p < 0.01$) in all three Zones except the diatomaceous ooze sediments (not correlated). TIC and band depth at 4.0 μm (associated with carbonate) are strongly correlated (positive coefficient significant at $p < 0.01$) in all three Zones except for diatomaceous ooze sediments (not correlated). This fits with results from previous works that have demonstrated the utility of VNIR reflectance spectra in this system as a way to rapidly assess sediment composition (Goudge et al., 2017; Sheppard et al., 2019; Weber et al., 2015). Although this has been shown previously in cores, here we demonstrate that the patterns in modern surface sediment continue with depth, such that diagenetic alteration, changing sediment sources, etc. do not fundamentally alter the relationships between chemistry and mineralogy nor the application of the tool.

Given the distinct mineralogical and chemical changes seen in the core, it is important to consider patterns and relationships in mineralogy and chemistry independently within each of the three Zones. An example of this is the relationship between Fe and Ti (Figure 5a, Table S7). Ti is an important element in the Towuti system and has been used as a proxy for increased physical weathering and runoff due to an increase in the detrital influx of rutile and/or ilmenite under those conditions (Russell et al., 2014). There is no clear correlation between FeO and TiO_2 abundance for the core samples as a whole, but when separated by zone it becomes apparent that there is no correlation in Zone 3, a strong positive correlation in Zone 2 (positive coefficient significant at $p < 0.01$), and a strong negative correlation in Zone 1 (negative coefficient significant at $p < 0.01$). SiO_2 and TiO_2 abundances are similarly complex (Figure 5b and Table S8) and exhibit a positive correlation in Zone 3 (positive coefficient significant at $p < 0.05$), no correlation in Zone 2, and a strong positive correlation in Zone 1 (positive coefficient significant at $p < 0.01$). A positive correlation between Si and Ti was also observed and previously reported for the lake surface sediment samples (Sheppard et al., 2019).

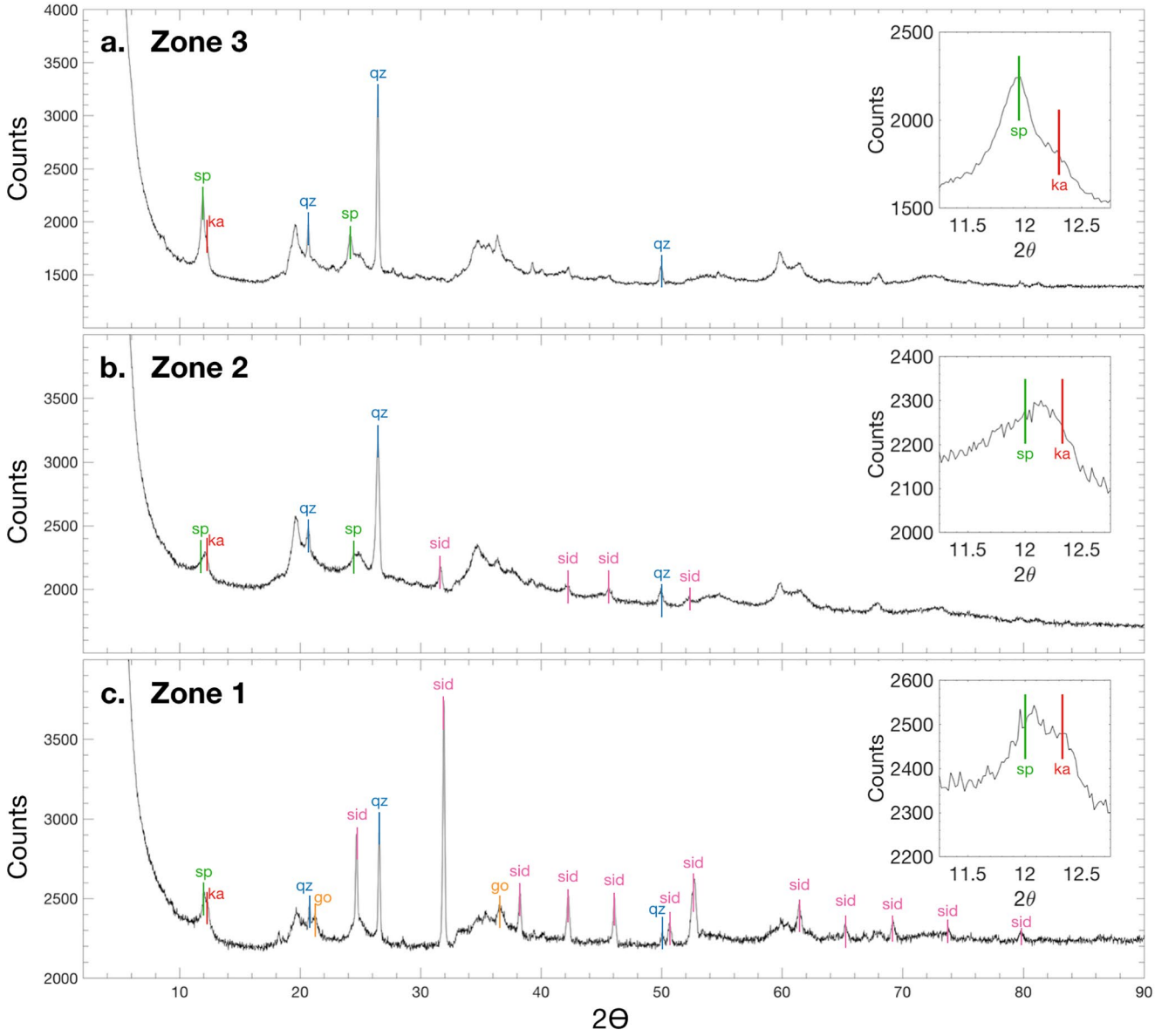

Figure 6. X-ray diffraction pattern of representative samples from (a) Zone 3, (b) Zone 2, and (c) Zone 1. Insets show the ~7 Å peak used to identify serpentine and kaolinite. (sp, Mg-serpentine; ka, kaolinite; qz: quartz; go, goethite; sid, siderite).

4.2. X-Ray Diffraction

XRD patterns of samples from the three Zones are consistent with the spectral and bulk elemental results discussed above (Figure 6). The dominant minerals in Zone 3 are quartz and serpentine, with lesser amounts of kaolinite. XRD patterns for Zone 2 samples are consistent with decreased serpentine content; kaolinite is as abundant or slightly more abundant than serpentine; siderite is present in some samples. Patterns for Zone 1 samples indicate this portion of the composite core is characterized by siderite, quartz, serpentine, kaolinite, and goethite. Our identification of the carbonate as siderite based on spectral characteristics is supported by microscopic identifications and by the absence of other carbonate minerals in the XRD patterns. Importantly, there were very few occurrences of crystalline Fe oxides in XRD data despite the catchment bedrock often being topped by well developed lateritic soils and abundant goethite, hematite, and magnetite. This is consistent with the Mössbauer data (see below) that indicate a significant portion of the Fe is associated with nanocrystalline or X-ray amorphous phases.

We note Fe fluorescence from the Cu XRD source has likely raised the counts background in these patterns, including possibly the steep rise in counts at low angles 2θ; this process will not affect the location or intensity of peaks used for mineral identification (Mos et al., 2018).

4.3. Mössbauer Spectroscopy

The Mössbauer spectra indicate the samples are mineralogically complex with respect to Fe^{2+} and Fe^{3+}. There appears to exist a significant amount of nanocrystalline material that contains both ferrous and ferric iron. Example Mössbauer spectra and their fits are presented in Figure 7 for two samples from Zone 3. The first sample (Figures 7a–7c) is green in color and comes from a depth of 1.35 mcd. The spectrum acquired at 295 K exhibits two ferrous and two ferric doublets. One of the ferric doublets has an IS above 0.5, which may indicate admixing of ferrous iron through exchange processes. At 130 K, these four doublets are still present and a sextet becomes visible (light blue in Figure 7). The wide spacing of the sextet suggests the presence of hematite. At 4 K there is evidence of an unknown ferrous phase. There is also a high IS sextet that could be indicative of the ferrous Fe in magnetite undergoing magnetic ordering. If magnetite is present it is likely very fine-grained. Other sextets observed at 4 K are typical of poorly ordered or fine-grained oxides (e.g., hematite, goethite, akaganeite, or a mix).

The second sample (Figures 7d–7f) is red in color and comes from a depth of 6.87 mcd. The spectrum acquired at 295 K also exhibits two ferrous and two ferric doublets. These are not particularly diagnostic but are consistent with Fe in smectite. At 130 K, the IS for both ferrous doublets increases appreciably but the QS increases only modestly. This is consistent with a magnetically split phase that could be hematite, goethite, or akaganeite. Spectra of the sample become increasingly complex when measured at 4 K, for which ~47% of the spectral area is consistent with nanophase (oxyhydr)oxide-like materials.

4.4. Color

For all three Zones, the characteristic chemical and mineralogical signatures (Mg-serpentine, Al-clay minerals, and TIC/siderite) appear to be only weakly related to the wet sediment color (red vs. green). Oxidation state and coordination state of Fe is likely the dominant source of red and green color variations due to electronic absorption processes such as charge transfer and/or crystal field splitting. However, Fe does not have to be hosted in crystalline phases. The abundance of amorphous Fe in the lake sediment can therefore lead to partial decoupling of sediment color from crystalline Fe mineralogy. The core sediments are rich in Fe (FeO up to ~30 wt%) and their corresponding reflectance spectra exhibit clear Fe absorptions at visible and NIR wavelengths. These spectral characteristics are strongly correlated with FeO content (positive coefficient significant at $p < 0.01$) in all three drill core Zones (Figure 8a and 8b, Tables S5 and S6). This indicates that both of the spectral parameters related to Fe absorptions (at 0.48 and 0.90 μm) are good proxies for Fe abundance. However, Fe abundance and the abundance of specific Fe minerals do not exhibit a unique correlation with sediment color. Both red and green sediment span a range of Fe abundances (Figures 8c and 8d). Furthermore, the relationship between wet color, dry color, and Fe host is complex (Figure 9). The samples with siderite are often red in appearance, whereas those that lack siderite are commonly green; however, we do observe exceptions to this pattern. Some of the red samples exhibit no clear evidence for siderite in the XRD or IR data, and siderite is observed in XRD patterns of several green samples. Importantly, some of these exceptions are observed for samples whose color was the same in all four indices (qualitative and quantitative assessments for both wet and dry cases), indicating sample handling does not influence this result.

4.5. Summary of Elemental and Mineralogical Trends With Depth

Statistical analyses of the spectral reflectance data identify two significant breaks or three distinct Zones in the Site 1 composite drill core (Supporting Information, Figures 1 and 2). Each of these Zones also exhibit clear differences in the independently measured elemental and mineralogical (XRD) data (Figure 4). Zone 1 (97–62 mcd) is dominated by carbonate (siderite) features in the spectral and elemental (TIC) data, with evidence of kaolinite and lesser serpentine. XRD patterns show that the non-siderite crystalline mineralogy of Zones 1 and 2 are quite similar, dominated by kaolinite with some serpentine and a small amount of

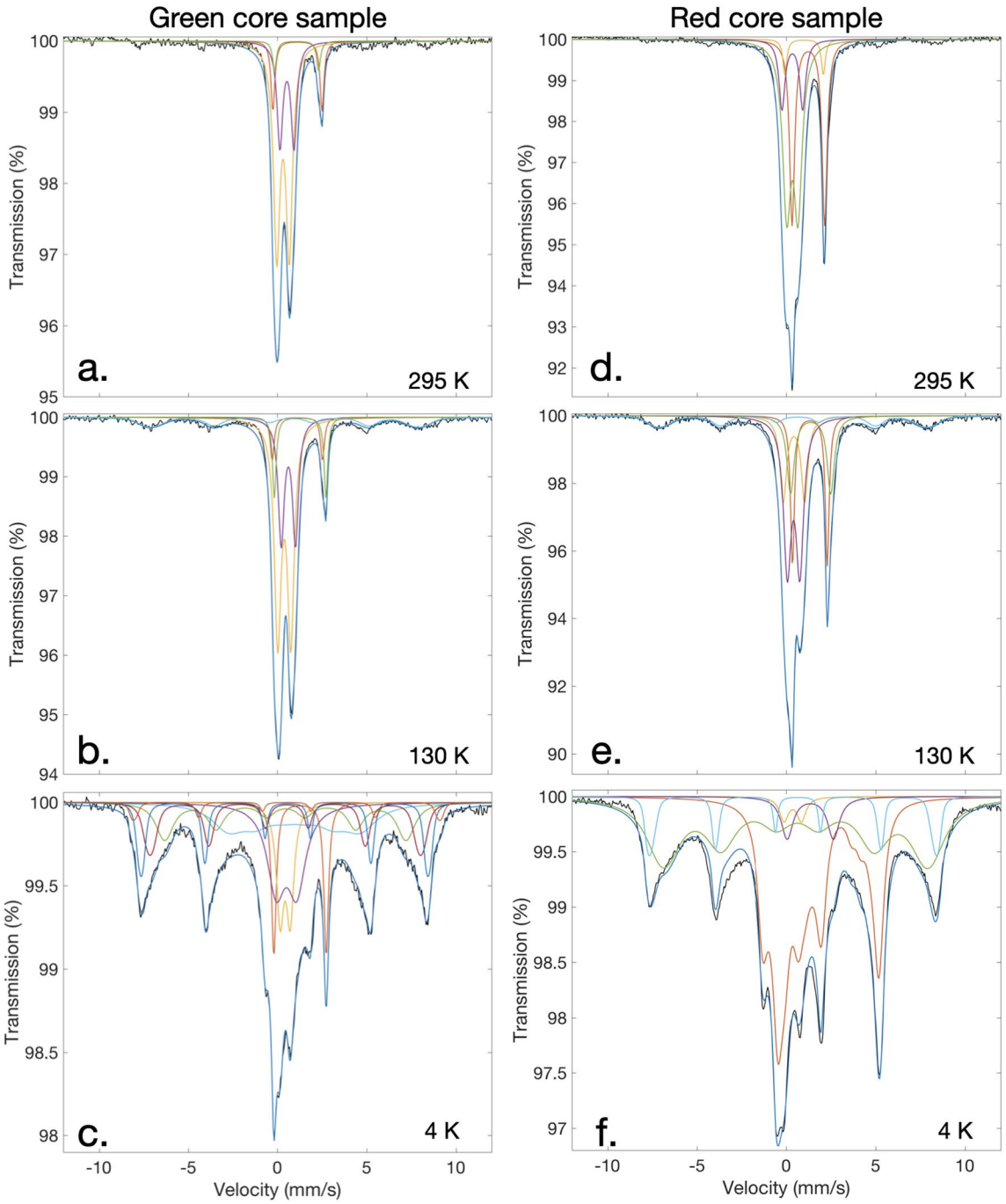

Figure 7. Mössbauer spectra and fits of a green section of Zone 3 at (a) 295 K, (b) 130 K, and (c) 4 K. Mössbauer spectra and fits of a red section of Zone 3 at (d) 295 K, (e) 130 K, and (f) 4 K.

crystalline Fe oxides. Across the boundary from Zone 1 to Zone 2, siderite content decreases and Al-clay mineral increases; Zone 2 also has two regions of diatomaceous ooze. Zone 3 (27–0 mcd) is dominated by Mg-serpentine with lesser amounts of Al-clay minerals (kaolinite, based on spectral and XRD data) and occasional occurrences of siderite. The transition at Zone 1–2 is relatively gradual, while that at Zone 2–3 is much sharper (Figure 4). The statistically defined visible-near IR spectral divisions (Zones 1–3) presented here are consistent with the subdivision of Unit 1 (1a–1c) described by Russell et al. (2020), which were qualitatively defined based on visual inspection of the sediment core and down-core variations in

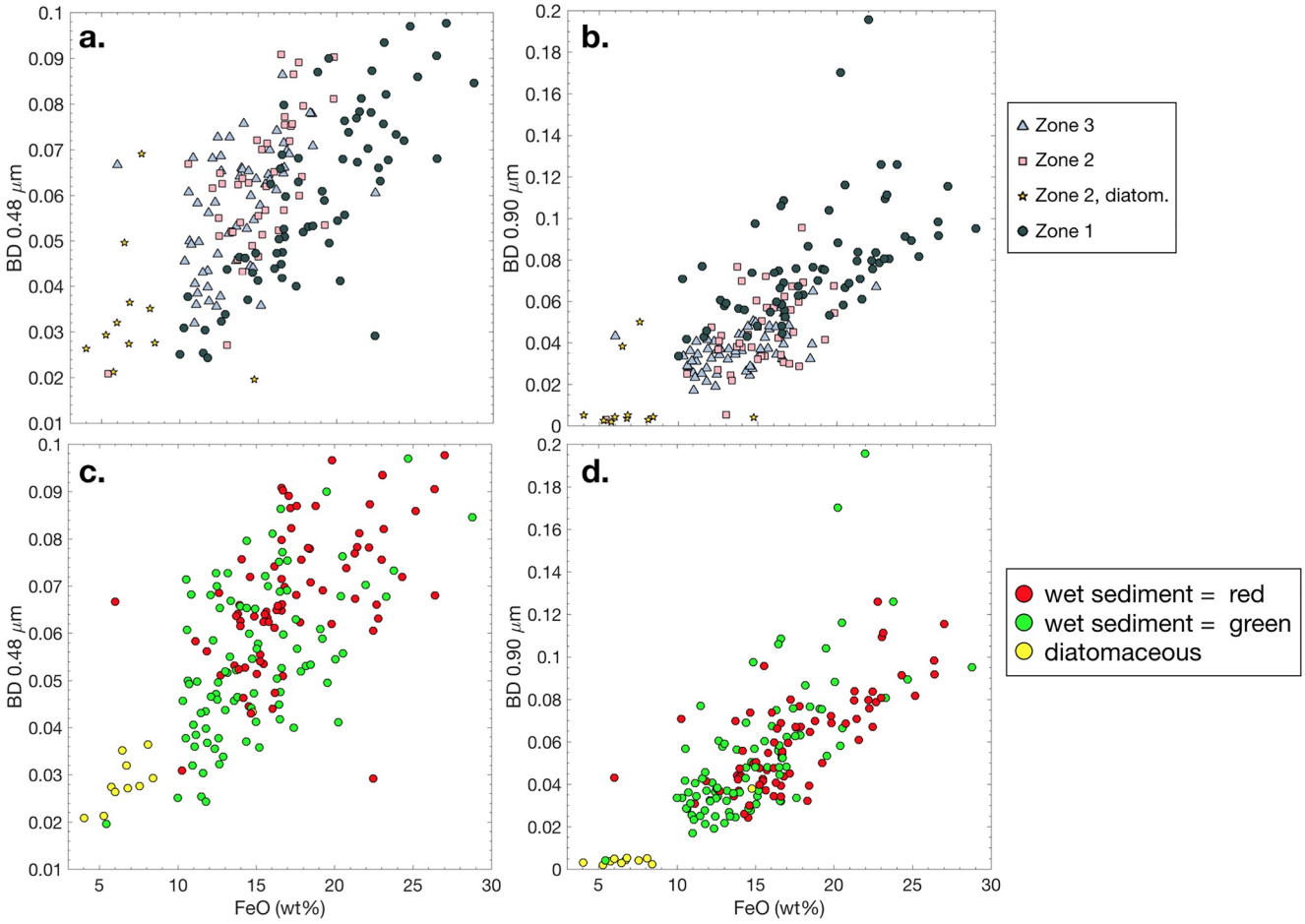

Figure 8. Band depth of two iron absorptions, 0.48 μm (a and c) and 0.9 μm (b and d), versus FeO abundance (wt%). Colored according to core Zone (a and b) or wet sediment color (c and d).

elemental abundance. The results of our study give statistical confidence, that these three sections of Unit 1 are compositionally distinct from each other, and that the compositional changes are linked to changes in mineralogy.

Fe_{total} is ~10–30 wt% in the non-diatomaceous sediments; although the highest Fe samples are all in Zone 1, many samples from Zones 3 and 2 also exhibit elevated FeO abundances (Figures 8a and 8b). The average FeO content is only slightly higher in red samples than in green, with both colors spanning the full range of FeO content (Figures 8c and 8d). Both red and green sediment exhibit a range of ferric and ferrous components, and the bulk of the iron appears to be associated with X-ray amorphous or poorly crystalline phases (Figure 7). These results are broadly consistent with the observations of Sheppard et al. (2019): whereas Fe in catchment sediments is mostly in the form of crystalline Fe oxides, by the time sediment has settled to the sediment/water interface, much of the Fe (>50% of the total Fe) is associated with X-ray amorphous phases. The most commonly identified ferrous phase in the XRD and VNIR data, siderite, is most often associated with red layers. This is consistent with the distribution of siderite described by Russell et al. (2020).

5. Discussion

The three Zones within the Lake Towuti Site 1 composite drill core are defined by changes in chemistry and mineralogy that are reliably detected using multiple techniques. We observe evidence for elevated abundance of Mg-serpentine (Zone 3, 27–0 mcd), elevated abundance of Al-clay minerals (Zone 2, 62–27 mcd), and elevated abundance of siderite (Zone 1, 97–62 mcd) in reflectance spectra, XRD, and elemental

Sample No.	Depth (mblf)	Wet Qual.	Wet Quant.	Siderite in VNIR	Siderite in XRD
294	0.07			no	
295	0.55			no	no
296	1.03			no	no
297	2.91			no	
298	3.38			yes	yes
299	3.86			no	yes
300	4.34			no	yes
301	4.99			yes	
302	5.39			no	
303	5.87			yes	
304	6.35			yes	
305	6.83			yes	
306	7.31			yes	
307	7.79			yes	
308	8.25			no	no
309	8.73			no	
310	9.21			no	
311	9.69			no	
312	10.17			no	
313	10.84			no	
314	11.61			yes	yes
315	12.09			yes	yes
316	12.56			yes	
317	13.04			yes	
318	13.52			no	
319	14.14			no	
320	14.62			no	
321	15.10			no	no
322	15.57			no	
323	16.05			no	
324	16.52			yes	yes
325	17.06			no	no
326	17.43			no	
327	17.91			no	no
328	18.87			yes	
329	19.34			no	
330	19.86			no	
331	20.25			no	
332	20.73			yes	
333	21.20			yes	yes
334	21.67			yes	
335	22.15			no	
336	22.62			no	
337	22.82			no	
338	23.29			no	
339	23.77			no	
340	24.24			no	
341	24.72			no	
342	25.19			no	
343	25.81			no	
344	26.14			no	
345	26.61			no	

Sample No.	Depth (mblf)	Wet Qual.	Wet Quant.	Siderite in VNIR	Siderite in XRD
353	29.99			no	
354	30.46			no	no
355	30.93			yes	
356	31.34			yes	
357	33.37			no	
358	33.85			no	
359	34.32			no	no
360	34.84			no	
361	35.23			no	
362	35.71			no	
363	36.19			no	
364	36.67			no	
365	37.15			no	
366	37.62			yes	yes
367	38.08			yes	
368	38.55			no	
369	39.01			no	
370	39.48			no	
371	39.95			no	no
372	41.01			yes	
373	41.34			yes	
374	41.81			yes	
375	42.30			yes	
376	42.77			yes	
377	43.25			no	no
378	44.14			no	
379	44.62			no	
380	45.09			no	
381	46.53			no	
382	47.01			no	
383	47.49			no	
384	47.97			no	
385	48.45			no	no
386	48.93			no	
387	49.25			yes	
388	49.72			yes	
389	50.69			yes	
390	51.16			yes	
391	51.64			no	
392	52.11			no	no
393	52.58			no	
394	53.04			no	
395	53.53			no	
396	54.00			no	no
397	54.46			yes	
398	55.48			no	
399	55.90			no	
400	56.21			no	
401	56.49			no	yes
402	56.97			no	
403	57.44			yes	
404	57.91			no	no
405	58.38			yes	
406	58.86			no	yes
407	59.33			yes	
408	59.69			no	no
409	60.28			yes	
410	60.77			yes	
411	61.69			yes	
412	62.17			yes	
413	62.68			yes	
414	63.16			yes	

Sample No.	Depth (mblf)	Wet Qual.	Wet Quant.	Siderite in VNIR	Siderite in XRD
415	63.63			yes	
416	64.10			yes	
417	64.58			no	
418	65.05			no	no
419	65.37			yes	
420	65.85			no	
421	66.78			yes	
422	67.26			yes	
423	67.73			no	
424	68.34			yes	no
425	68.70			no	
426	69.31			yes	yes
427	69.66			yes	yes
428	70.13			no	
429	70.61			yes	yes
430	71.09			yes	
431	71.59			yes	
432	72.16			yes	
433	72.64			yes	
434	73.11			no	
435	73.59			no	no
436	74.07			no	
437	74.94			yes	yes
438	75.42			yes	
439	75.90			yes	
440	76.37			yes	
441	76.62			yes	
442	77.32			yes	
443	78.48			yes	
444	78.96			yes	
445	79.43			no	
446	79.91			yes	
447	80.38			yes	
448	80.80			yes	
449	81.27			yes	
450	81.75			yes	
451	82.21			yes	
452	82.70			yes	yes
453	83.18			yes	
454	84.01			yes	
455	84.49			yes	
456	84.97			yes	yes
457	85.45			yes	
458	85.93			yes	yes
459	86.40			no	no
460	87.38			yes	
461	87.85			yes	
462	88.32			yes	
463	88.79			no	
464	89.26			no	no
465	89.75			yes	
466	90.24			yes	
467	90.71			yes	
468	91.18			yes	
469	91.64			no	
470	92.10			no	
471	92.58			no	no
472	92.99			no	
473	93.46			yes	
474	93.93			yes	
475	94.41			yes	
476	94.88			yes	yes
477	95.35			yes	
478	95.86			no	no

Figure 9. Data on wet sample color for the three Zones (Zone 3 left, Zone 2 center, Zone 1 right). Qualitative color is based on optical analysis of the freshly cut cores at LacCore. Quantitative color is based on white-balanced RGB data collected from freshly cut cores by the core scanner at LacCore. Presence of siderite in visible-near infrared is based on a perceptible 4.0 μm CO_3 band. Presence of siderite in X-ray diffraction is based on a peak at 32° 2θ.

abundance data. The data presented here demonstrate that spectral characteristics at VNIR wavelengths are well correlated with sediment bulk chemistry throughout the core and can accurately distinguish between different clay minerals (e.g., Al- vs. Mg-rich), carbonates, and total Fe content, similar to trends previously reported for the modern surface sediments (Goudge et al., 2017; Morlock et al., 2018; Sheppard et al., 2019; Weber et al., 2015). However, due to the complex nature of Fe mineralogy within Lake Towuti, other methods must be used to investigate the specific hosts and oxidation state of Fe. Mössbauer and XRD analyses suggest that Fe in the drill core sediment is hosted in a variety of phases, mostly nanocrystalline and/or X-ray amorphous, and includes both ferrous and ferric phases. We also note that freeze-drying saturated solutions has led to precipitation of amorphous phases (Ihli et al., 2013), which may account for some of the amorphous phases we observe, although the depth-dependence of amorphous phase abundance (Sheppard et al., 2019) implies that not all the amorphous phases seem to be related to this process.

5.1. Environmental Variations Reflected in Core Sediments

The boundary between Zone 1 and Zone 2 is characterized by a substantial decline in siderite. Both red and green beds are observed in both Zones 2 and 1, and Zone 1 is slightly redder overall. XRD patterns show that the non-siderite component of these Zones is quite similar, dominated by kaolinite with a smaller component of serpentine and small amount of crystalline Fe oxides. Furthermore, much of the siderite in Zone 1 occurs in the form of nodules (Russell et al., 2020). From this, we conclude that the sediment sources for Zones 2 and 1 are similar in that the detrital silicates are dominated by Al-rich clay minerals. The increase in siderite abundance in Zone 1 relative to the overlying Zone 2 is likely a result of progressive carbonate nodule growth during burial diagenesis (e.g., Vuillemin et al., 2019). In contrast, Zone 3 is dominated by coarser-grained Mg-serpentine-rich sediment, similar to what composes the currently prograding Mahalona delta (Costa et al., 2015; Goudge et al., 2017; Vogel et al., 2015). This delta material originates from the serpentine-rich mafic bedrock the Mahalona is currently incising (Costa et al., 2015; Tamuntuan et al., 2015) and is distinct from the Al-rich silicates observed in Zones 1 and 2. Both red and green sediment is seen in Zone 3, although sediment is greener than Zones 2 and 1.

The similarity between Zones 2 and 1, and the distinct changes in clay mineralogy relative to Zone 3, indicate that there are two primary depositional regimes (Zones 3 and 1/2) represented in the Site 1 composite drill core (Russell et al., 2020). Super-imposed over the signature of the older depositional setting (Zones 1/2), there is a strong diagenetic signal related to burial of reactive iron and growth of siderite (differentiating Zone 2 and the more diagenetically influenced Zone 1). Currently, and in the recent past, the Mahalona River has dominated sediment deposition in the northern basin of Lake Towuti (e.g., the region influenced by the Mahalona delta). The climate is such that the Mahalona river has continued to incise and transport the local serpentinized bedrock, resulting in the deposition of coarser Mg-rich sediment into the lake. The second regime, corresponding to Zones 2 and 1, represents an older period of time (likely hundreds of thousands of years, based on estimated sedimentation rates) when the role and/or existence of the Mahalona river must have been fundamentally different. In this regime, the sediments deposited in the northern basin of Lake Towuti were enriched in Al-clay minerals and Fe-phases (likely Fe-oxy/hydr/oxides), an assemblage that is more consistent with erosion, transport, and deposition of deeply weathered soil profiles (e.g., laterites) in the catchment. We note that carbonate is present throughout the composite core, indicating crystallization can occur shortly after deposition, but the increase in carbonate abundance with depth coincides with an increase in the appearance of larger carbonate nodules. The nodular appearance of the siderite likely reflects long-term diagenesis. The Zone 1–2 transition is also relatively diffuse, which is consistent with a diagenetic origin as such nodules take time to grow during burial. The increased frequency of siderite beds, and the decoupling of TIC from TOC (Russell et al., 2020) likely reflects a more frequently oxidizing and more productive lake, meaning it may have been shallower in that period (Zone 1) as well. The combination of these two factors (structural and diagenetic) lead to a Zone 1 greatly enriched in siderite. This change in environment at the Zone 1–2 boundary may also be the source of the changing statistical relationship between Fe and Ti (Figure 5a). These elements are strongly negatively correlated in Zone 1, uncorrelated in Zone 2, and weakly positively correlated in Zone 3. The observation of this changing relationship at the Zone 1–2 boundary demonstrates the applicability of Simpson's paradox to sedimentary studies; to properly assess elemental relationships within a sedimentary system, the proper sedimentary boundaries between depositional regimes must be applied.

The striking differences between Zones 3 and 1–2 can be considered through the lens of from where in a weathering column the material was sourced based on dominant erosion and transport processes at the time (Figure 10). In a standard soil weathering profile (Nesbitt et al., 1997), especially in the tropics where water is abundant, chemical weathering will outpace physical weathering in areas of low topographic relief, leading to soil profiles with finer-grained secondary weathering products at the top (e.g., clay minerals, gibbsite, and Fe oxy/hydr/oxides) and coarser-grained bedrock fragments at the bottom. We propose that Zone 3 at the top of the composite core is sourced from the base of this idealized weathering profile, with abundant coarser-grained Mg-serpentine from the catchment bedrock and lesser amounts of mature chemical weathering products such as Al-rich clay minerals. In contrast, weathering products in Zones 1–2 are dominated by Al-clay minerals and nanophase Fe oxides, similar to what is expected for the upper section of an idealized weathering profile, farther from the bedrock. The Zone 2–3 transition is also relatively sharp, with an

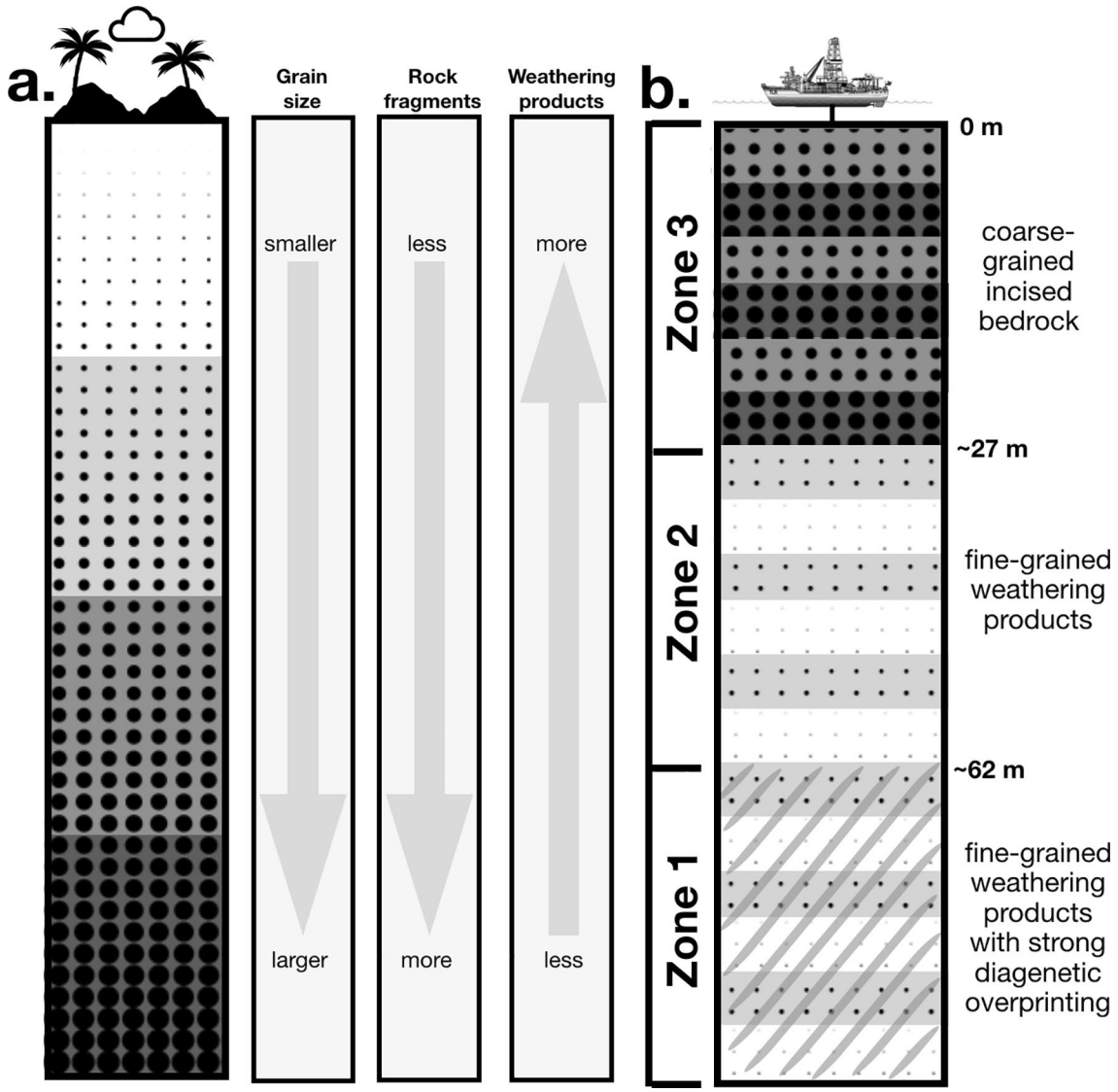

Figure 10. (a) A theoretical weathering profile, showing how grain size, abundance of coarse rock fragments, secondary weathering products, and diagenetic overprinting are related to depth, in part based on Nesbitt et al. (1997). (b) Schematic of the Site 1 composite drill core, showing from where in the idealized weathering profile that Zone's sediments were likely sourced. Zone 3 is likely sourced from lower in the weathering profile, coarser-grained bedrock; Zone 2 is likely sourced from higher in the weathering profile, dominated by fine-grained secondary weathering products like clay minerals and Fe oxides; Zone 1 is likely sourced from a similar part of the weathering profile as Zone 2 but is overprinted by a longer duration of diagenetic processes.

abrupt increase in Mg-serpentine within 1–2 m. This is consistent with a structural cause that would quickly change the conditions of the major inlet and thus the sediment source to this part of the lake. Russell et al. (2020) describes how the onset of the strong influence of the Mahalona River and the associated delta (what we label here the transition from Zone 2 to Zone 3) is likely caused by a river capture event linking the Lampenisu and Mahalona Rivers. Consistent with this, these changes at the Zone 2–3 transition appear to be related to the large scale evolution of the basin and river system as a whole rather than a significant shift in climatic conditions and/or change in the rate of chemical weathering in the sediment source region. The positive correlation between Si and Ti (Figure 5b) in Zones 1 and 3 is consistent with the correlation between these elements observed in Towuti surface sediment samples (Sheppard et al., 2019) and is consistent with interpretations that an increase in Ti can be used as a proxy for increased physical weathering during runoff in the source region, leading to an increase in detrital rutile and/or ilmenite (Russell et al., 2014).

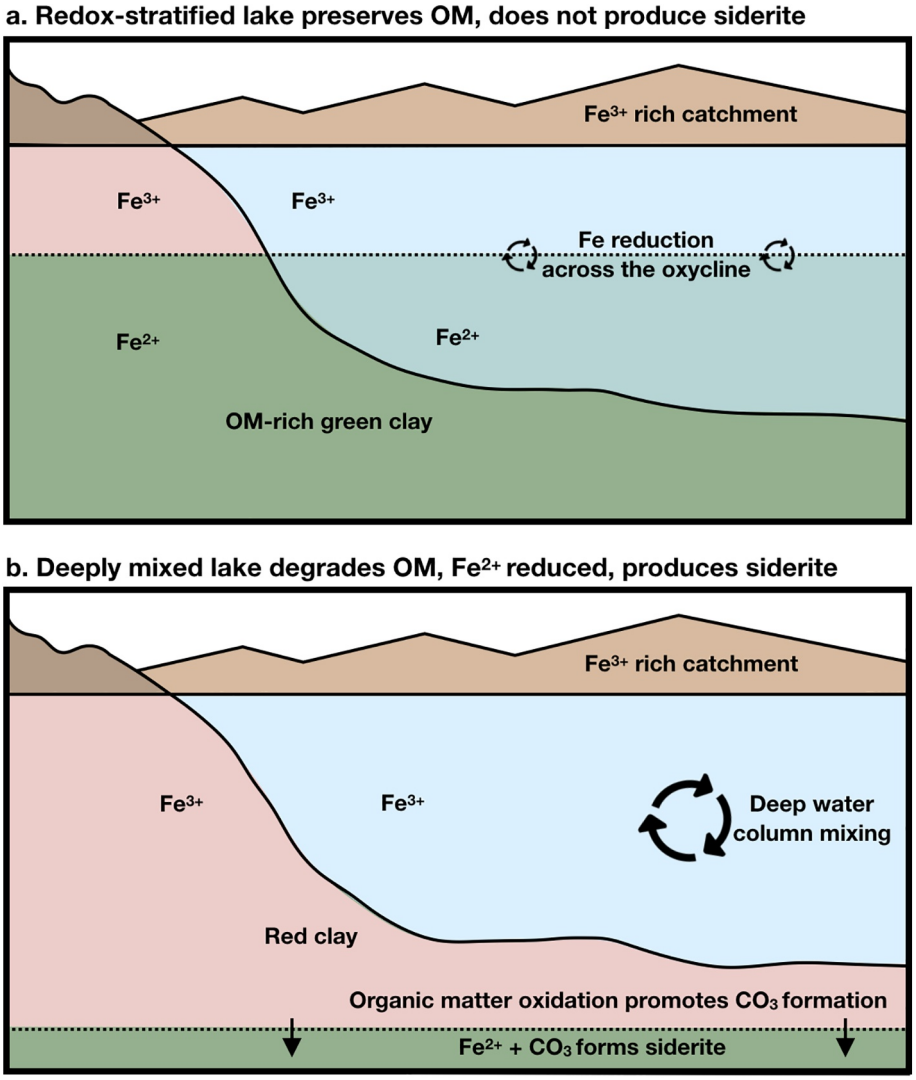

Figure 11. Schematic of the lake during times of (a) redox stratification and (b) deep mixing.

5.2. Oxidation State of Lake Towuti Through Time

The alternating pattern of red and green clays may provide a proxy for understanding past variations in lake stratification, temperature, and lake depth, and their impacts on oxidation state of the bottom water. This proposed link can be seen in Figure 11. During times of thermal and redox stratification, including present-day (Costa et al., 2015), Fe^{3+} (likely particulate oxides and amorphous phases) is stable in the water column and adjacent pore space above the oxycline, while Fe^{2+} (likely dissolved) is stable in the water column and pore space below the oxycline. During periods of redox stratification, Fe cycling across the oxycline encourages incorporation of Fe into amorphous phases (Sheppard et al., 2019; Vuillemin et al., 2019), and sediment along most of the lake bottom is rich in ferrous minerals, clay minerals, and organic matter. During mixing events, Fe^{3+} is stable throughout the water column and adjacent pore space. This creates a flux of reactive Fe^{3+} to the lake bottom, and organic material in sediment along the lake bottom is expected to degrade quickly under these oxidizing conditions, providing a source of CO_3. Below some depth, the sediment and associated pore fluids transition to a reducing environment that favors conversion of Fe^{3+} to Fe^{2+}. These conditions ultimately favor the formation of siderite, and with increasing burial depth and/or time the siderite nuclei grow to form the large and abundant siderite nodules found deeper in Zone 1 (Russell et al., 2020; Vuillemin et al., 2019).

Although this model seems likely to explain many of the lithologic changes in Lake Towuti, our findings suggest that the Fe mineralogy of the composite core is extremely complex and includes both ferrous and ferric Fe remaining in amorphous components even deep in Zone 1. Furthermore, though many of the red clay mineral-rich layers contain siderite, a number of red layers lack evidence for siderite and many green sediments are found to contain siderite. Therefore, while Figure 11 presents a useful environmental scheme, the proposed reactions may not have gone to completion in all cases. This also indicates that the visible color (i.e., red vs. green) of clay layers is not a perfect predictor of oxidation state (i.e., Fe^{2+} vs. Fe^{3+}) or siderite presence. The Fe host is sufficiently complex and difficult to characterize, in part due to the significant amorphous fraction that has evidence for both ferrous and ferric Fe, that redness cannot be used as a reliable proxy for Fe mineralogy, including siderite content.

Our findings suggest that there are at least two possibilities for what is the first order driver of sediment color: (a) the ferrous Fe carbonate siderite or (b) ferrous and/or ferric Fe hydr/oxides that are nanocrystalline/poorly crystalline. The XRD and VNIR/Mössbauer spectral analyses indicate that many of the reddest samples are indeed enriched in siderite, but there are enough samples that are red with no siderite or green with siderite to suggest that siderite content may not always be the main determinant of sediment color. Furthermore, siderite can under certain conditions appear as other colors including green, gray, and yellow (Lavina et al., 2009; Taran et al., 2017). The most parsimonious explanation is that a combination of Fe-bearing minerals (carbonate, serpentine, and nanophase hydr/oxides) and amorphous Fe-rich materials result in multiple overlapping absorptions at visible wavelengths that give rise to the observed red and green sediment color. Similar to what was observed for the modern surface sediments (Sheppard et al., 2019), Mössbauer analyses of the core samples indicate they often contain a complex assemblage of ferrous and ferric components. As such, sediment color is not at this time a reliable proxy for mineralogy or redox state of Fe in the sediment. While the red sediment has, on average, lower TOC (Russell et al., 2020), higher Fe, and more siderite, we are unable to say that color indicates the presence of a specific mineral suite, particularly for the Fe minerals. The bulk sediment composition does indicate deposition under oxidizing conditions (e.g., bottom water and/or pore space oxidation), but given the complex mineralogy of Fe inputs and postdepositional cycling, there is no perfectly consistent relationship between sediment color and Fe mineralogy. Sediment color is likely more an indication of the extent and effectiveness of redox conditions and/or organic C availability than a particular mineral assemblage. Future studies that focus on a more detailed characterization of the nanocrystalline Fe mineralogy and relative proportions of Fe^{2+}/Fe^{3+} in the original, wet sediment are warranted.

In light of these findings, the gradual transition from Zone 1 to Zone 2 could result from a variety of different environmental processes, including climatic changes that affect water column stability, and/or the gradual tectonic subsidence of the lake floor that increases lake depth. Alternatively, this zonation could reflect in part the slow rate of diagenetic chemical transformations occurring in the sediment, with the reactions in Zone 1 being "more complete" than in Zone 2. In short, this transition reflects a combination of surface environmental and sub-surface diagenetic processes that affect the availability of Fe and CO_3.

6. Conclusions

We identify and describe three distinct Zones in the Lake Towuti Site 1 Composite Core. Zone 1 (97–62 mcd) is characterized by Al-bearing clay minerals such as kaolinite and abundant siderite, Zone 2 (62–27 mcd) is dominated by kaolinite with lower abundances of siderite, and Zone 3 (27–0 mcd) is dominated by Mg-serpentine and the least amount of siderite. Each identified zone contains both red and green clay-rich sediment, the color of which is influenced by siderite (most common in Zone 1) as well as complex, Fe-bearing, mixed-valence, X-ray amorphous components. VNIR spectral parameters are strongly correlated with elemental abundances in the sediment samples, confirming that reflectance spectroscopy can be used as a rapid, remote technique for assessing sediment composition in both old and modern sediments in the Towuti system, as well as other lake basins with mafic sources.

The transition in clay mineralogy from Mg-rich serpentine to Al-rich clays at a depth of 27 mcd (Zone 2–3) indicates a major change in the type of detritus supplied to the lake. The younger Mg-rich beds are consistent with transport of coarser, relatively unweathered materials from the surrounding bedrock, whereas the

older Al-rich sediments are more consistent with transport and deposition of material sourced from better developed weathering profiles. Although the clay mineralogy in the composite core is interpreted to record information about the evolution of the sediment source region, diagenetic processes associated with redox cycling of Fe strongly affect the sediment composition, particularly in deeper sections of the succession. This is indicated by the persistence of abundant ferrous and ferric nanophase and X-ray amorphous phases throughout the core and an increase in the abundance and size of siderite nodules with depth. It is likely that siderite nodules in Zone 1 are still forming from remaining reactive Fe in the poorly crystalline components that originally formed near the sediment-water interface shortly after sediment deposition (e.g., Sheppard et al., 2019). The persistence of amorphous material in Zone 1 sediment, even as it is converted to siderite nodules, may imply a greater amount of reactive Fe initially buried during this time period when the lake was likely shallower and more oxidizing.

Finally, we find that Fe-rich amorphous material is abundant in both red and green clay layers and includes ferrous and ferric components. This complicates the use of sediment color as a unique indicator of Fe oxidation state for different layers in the composite core. Though siderite is most commonly associated with red clay layers, future studies that utilize methods capable of characterizing the oxidation state of Fe in the nanocrystalline and amorphous components, the quantitative abundance of these amorphous materials, and how these relate to organic components, are warranted to fully understand how best to reconstruct paleo redox conditions in Lake Towuti.

Data Availability Statement

The spectral, chemical, and XRD data used in this study are publicly available on Pangaea.de at https://doi.org/10.1594/PANGAEA.932877. This study was done as a private venture and not in the author's capacity as an employee of the Jet Propulsion Laboratory, California Institute of Technology.

Acknowledgments
Funding for laboratory experiments were provided by Brown University Presidential Fellowship and NASA Astrobiology Institute (MIT team, award NNA13AA90A). Sample collection during the Towuti Drilling Project was supported by grants from the International Continental Scientific Drilling Program (ICDP), the US National Science Foundation (NSF-EAR #1401448), the German Research Foundation (DFG; ME 1169/26), the Swiss National Science Foundation (SNSF; 20FI21_153054/1 & 200021_153053/1&2), Brown University, Genome British Columbia, and the Ministry of Research, Technology, and Higher Education (RISTEK). PT Vale Indonesia and the US Continental Drilling Coordination Office are acknowledged for the logistical assistance to the project. This research was carried out with permission from RISTEK, the Ministry of Trade of the Government of Indonesia, the Natural Resources Conservation Center (BKSDA), and the Government of Luwu Timur of Sulawesi. Mössbauer analyses were funded by Brown University SSERVI. The authors are very grateful to D. Murray and J. Orchardo for assistance with the ICP-AES. Grant Rutherford and Sarah Martinez assisted in laboratory work and data collection. Sample material was provided in part by the National Lacustrine Core Facility (LacCore). The authors are grateful to E. Rampe, R. Smith, and an anonymous reviewer for extremely helpful comments that improved the quality of this manuscript.

References

Bai, J., & Perron, P. (1998). Estimating and testing linear models with multiple structural changes. *Econometrica*, *66*(1), 47–78. https://doi.org/10.2307/2998540

Bai, J., & Perron, P. (2003). Computation and analysis of multiple structural change models. *Journal of Applied Econometrics*, *18*(1), 1–22. https://doi.org/10.1002/jae.659

Benson, T. R., & Mahood, G. A. (2016). Geology of the mid-Miocene rooster comb caldera and lake Owyhee volcanic field, eastern Oregon: Silicic volcanism associated with Grande Ronde flood basalt. *Journal of Volcanology and Geothermal Research*, *309*, 96–117. https://doi.org/10.1016/j.jvolgeores.2015.11.011

Bishop, J. L., Lane, M. D., Dyar, M. D., & Brown, A. J. (2008). Reflectance and emission spectroscopy study of four groups of phyllosilicates: Smectites, kaolinite-serpentines, chlorites and micas. *Clay Minerals*, *43*(1), 35–54. https://doi.org/10.1180/claymin.2008.043.1.03

Burns, R. G. (1993). *Mineralogical applications of crystal field theory*. Cambridge University Press.

Clark, R. N., King, T. V. V., Klejwa, M., Swayze, G. A., & Vergo, N. (1990). High spectral resolution reflectance spectroscopy of minerals. *Journal of Geophysical Research*, *95*(B8), 12653–12680. https://doi.org/10.1029/jb095ib08p12653

Clark, R. N., & Roush, T. L. (1984). Reflectance spectroscopy: Quantitative analysis techniques for remote sensing applications. *Journal of Geophysical Research*, *89*(7), 6329–6340. https://doi.org/10.1029/jb089ib07p06329

Colin, F., Nahon, D., Trescases, J. J., & Melfi, A. J. (1990). Lateritic weathering of pyroxenites at Niquelandia, Goias, Brazil: The supergene behavior of nickel. *Economic Geology*, *85*, 1010–1023. https://doi.org/10.2113/gsecongeo.85.5.1010

Costa, K. M., Russell, J. M., Vogel, H., & Bijaksana, S. (2015). Hydrological connectivity and mixing of lake Towuti, Indonesia in response to paleoclimatic changes over the last 60,000 years. *Palaeogeography, Palaeoclimatology, Palaeoecology*, *417*, 467–475. https://doi.org/10.1016/j.palaeo.2014.10.009

Dyar, D. M., Agresti, D. G., Schaefer, M. W., Grant, C. A., & Sklute, E. C. (2006). Mössbauer spectroscopy of earth and planetary materials. *Annual Review of Earth and Planetary Sciences*, *34*, 83–125.

Fristad, K. E., Pedentchouk, N., Roscher, M., Alexander, P., & Svensen, H. (2015). An integrated carbon isotope record of an end-Permian crater lake above a phreatomagmatic pipe of the Siberian traps. *Palaeogeography, Palaeoclimatology, Palaeoecology*, *428*, 39–49. https://doi.org/10.1016/j.palaeo.2015.03.010

Gaffey, S. J., McFadden, L. A., Nash, D., & Pieters, C. M. (1993). *Remote geochemical analysis: Elemental and mineralogical composition, chapter Ultraviolet, Visible, and Near-Infrared Reflectance Spectroscopy: Laboratory Spectra of Geologic Materials* (Vol. 43–78). Cambridge University Press.

Golightly, J. P., & Arancibia, O. N. (1979). The chemical composition and infrared spectrum of nickel- and iron-substituted serpentine from a nickeliferous laterite profile, Soroako, Indonesia. *The Canadian Mineralogist*, *17*, 719–728.

Goudge, T. A., Russell, J. M., Mustard, J. F., Head, J. W., & Bijaksana, S. (2017). A 40,000 yr record of clay mineralogy at Lake Towuti, Indonesia: Paleoclimate reconstruction from reflectance spectroscopy and perspectives on paleolakes on Mars. *GSA Bulletin*, *129*(7–8), 806–819.

Gudmundsdottir, E. R., Larsen, G., Bjorck, S., Ingolfsson, O., & Johan Striberger, J. (2016). A new high-resolution Holocene tephra stratigraphy in eastern Iceland: Improving the Icelandic and North Atlantic tephrochronology. *Quaternary Science Reviews*, *150*, 234–249. https://doi.org/10.1016/j.quascirev.2016.08.011

Hafidz, A., Bijaksana, S., Triyoso, W., Winardhie, I. S., Russell, J. M., Wattrus, N., et al. (2018). *Preliminary finding on the seismic stratigraphy of Lake Towuti, Indonesia*. American Geophysical Union.

Harder, H. (1976). Nontronite synthesis at low temperatures. *Chemical Geology*, *18*(3), 169–180. https://doi.org/10.1016/0009-2541(76)90001-2

Hasberg, A. K. M., Melles, M., Wennrich, V., Just, J., Held, P., Morlock, M. A., et al. (2018). Modern sedimentation processes in Lake Towuti, Indonesia, revealed by the composition of surface sediments. *Sedimentology*, *66*(2), 675–698. https://doi.org/10.1111/sed.12503

Ihli, J., Kulak, A. N., & Meldrum, F. C. (2013). Freeze-drying yields stable and pure amorphous calcium carbonate (ACC). *Chemical Communications*, *49*, 3134–3136. https://doi.org/10.1039/c3cc40807h

Kadarusman, A., Miyashita, S., Maruyama, S., Parkinson, C. D., & Ishikawa, A. (2004). Petrology, geochemistry and paleogeographic reconstruction of the East Sulawesi Ophiolite, Indonesia. *Tectonophysics*, *392*(1), 55–83. https://doi.org/10.1016/j.tecto.2004.04.008

Krivonogov, S. K., Yi, S., Kashiwaya, K., Kim, J. C., Narantsetseg, T., Oyunchimeg, T., et al. (2012). Solved and unsolved problems of sedimentation, glaciation and paleolakes of the Darhad basin, Northern Mongolia. *Quaternary Science Reviews*, *56*, 142–163. https://doi.org/10.1016/j.quascirev.2012.08.013

Lavina, B., Dera, P., Downs, R. T., Prakapenka, V., Rivers, M., Sutton, S., & Nicol, M. (2009). Siderite at lower mantle conditions and the effects of the pressure-induced spin-pairing transition. *Geophysical Research Letters*, *36*, L23306. https://doi.org/10.1029/2009gl039652

Morlock, M. A., Vogel, H., Nigg, V., Ordonez, L., Hasberg, A. K. M., Melles, M., et al. (2018). Climatic and tectonic controls on source-to-sink processes through space and time in a tropical ultramafic lake catchment: Lake Towuti, Indonesia. *Journal of Paleolimnology*, *61*(3), 279–295.

Mos, Y. M., Vermeulen, A. C., Cees, J., Buisman, N., & Jan, W. (2018). X-ray diffraction of iron containing samples: The importance of a suitable configuration. *Geomicrobiology Journal*, *35*(6), 511–517. https://doi.org/10.1080/01490451.2017.1401183

Nesbitt, W. H., Fedo, C. M., & Young, G. M. (1997). Quartz and feldspar stability, steady and non steady state weathering, and petrogenesis of siliciclastic sands and muds. *The Journal of Geology*, *105*(2), 173–192.

Russell, J., & Bijaksana, S. (2012). The Towuti drilling project: Paleoenvironments, biological evolution, and geomicrobiology of a tropical Pacific lake. *Scientific Drilling*, *21*, 29–40. https://doi.org/10.5194/sd-14-68-2012

Russell, J. M., Bijaksana, S., Vogel, H., Melles, M., Kallmeyer, J., Ariztegui, D., et al. (2016). The Towuti drilling project: Paleoenvironments, biological evolution, and geomicrobiology of a tropical Pacific lake. *Scientific Drilling*.

Russell, J. M., Vogel, H., Bijaksana, S., Melles, M., Deino, A., Abdul Hafidz, et al. (2020). The late quaternary tectonic, biogeochemical, and environmental evolution of ferruginous lake Towuti, Indonesia. *Palaeogeography, Palaeoclimatology, Palaeoecology*, *556*, 109905.

Russell, J. M., Vogel, H., Konecky, B. L., Bijaksana, S., Huang, Y., Melles, M., et al. (2014). Glacial forcing of central Indonesian hydroclimate since 60,000 y BP. *Proceedings of the National Academy of Sciences*, *111*(14), 5100–5105. https://doi.org/10.1073/pnas.1402373111

Sheppard, R. Y., Milliken, R. E., Russell, J. M., Darby Dyar, M., Sklute, E. C., Vogel, H., et al. (2019). Characterization of iron in Lake Towuti sediment. *Chemical Geology*, *512*, 11–30. https://doi.org/10.1016/j.chemgeo.2019.02.029

Sutter, B., Dalton, J. B., Ewing, S. A., Amundson, R., & McKay, C. P. (2007). Terrestrial analogs for interpretation of infrared spectra from the Martian surface and subsurface: Sulfate, nitrate, carbonate, and phyllosilicate-bearing Atacama Desert soils. *Journal of Geophysical Research*, *114*. https://doi.org/10.1029/2006jg000313

Tamuntuan, G., Bijaksana, S., King, J., Russell, J., Fauzi, U., Maryunani, K., et al. (2015). Variation of magnetic properties in sediments from Lake Towuti, Indonesia, and its paleoclimatic significance. *Palaeogeography, Palaeoclimatology, Palaeoecology*, *420*, 163–172. https://doi.org/10.1016/j.palaeo.2014.12.008

Taran, M. N., Müller, J., Friedrich, A., & Koch-Müller, M. (2017). High-pressure optical spectroscopy study of natural siderite. *Physics and Chemistry of Minerals*, *44*(8), 537–546. https://doi.org/10.1007/s00269-017-0880-7

Vogel, H., Russell, J. M., Cahyarini, S. Y., Bijaksana, S., Wattrus, N., Rethemeyer, J., & Melles, M. (2015). Depositional modes and lake-level variability at Lake Towuti, Indonesia, during the past 29 kyr BP. *Journal of Paleolimnology*, *54*(4), 359–377.

Vuillemin, A., Friese, A., Alawi, M., Henny, C., Nomosatryo, S., Wagner, D., et al. (2016). Geomicrobiological features of ferruginous sediments from Lake Towuti, Indonesia. *Frontiers in Microbiology*, *7*. https://doi.org/10.3389/fmicb.2016.01007

Vuillemin, A., Friese, A., Wirth, R., Schuessler, J. A., Schleicher, A. M., Kemnitz, H., et al. (2020). Vivianite formation in ferruginous sediments from Lake Towuti, Indonesia. *Biogeosciences*, *17*(7), 1955–1973. https://doi.org/10.5194/bg-17-1955-2020

Vuillemin, A., Wirth, R., Kemnitz, H., Anja Schleicher, A. M., Andre Friese, A., Bauer, K., et al. (2019). Formation of diagenetic siderite in modern ferruginous sediments. *Geology*, *47*, 540–544. https://doi.org/10.1130/G46100.1

Weber, A. K., Russell, J. M., Goudge, T. A., Salvatore, M. R., Mustard, J. F., & Bijaksana, S. (2015). Characterizing clay mineralogy in Lake Towuti, Indonesia, with reflectance spectroscopy. *Journal of Paleolimnology*, *54*(2), 253–261. https://doi.org/10.1007/s10933-015-9844-4

Widdowson, M. (2007). Laterite and ferricrete. In D. J. Nash, & S. J. McLaren (Eds.), *Geochemical sediments and landscapes* (pp. 46–94). Blackwell Publishing.